IEEE Access
Multidisciplinary | Rapid Review | Open Access Journal

Received 18 February 2024, accepted 12 March 2024, date of publication 18 March 2024, date of current version 22 March 2024.

Digital Object Identifier 10.1109/ACCESS.2024.3377560

RESEARCH ARTICLE

An Attention-Based Deep Learning Network for Predicting Platinum Resistance in Ovarian Cancer

HAOMING ZHUANG[1], BEIBEI LI[2], JINGTONG MA[1], PATRICE MONKAM[1], WEI QIAN[1], AND DIANNING HE[1]

[1]College of Medicine and Biological Information Engineering, Northeastern University, Shenyang 110057, China
[2]Department of Radiology, Shengjing Hospital of China Medical University, Shenyang 110004, China

Corresponding author: Dianning He (hedn@bmie.neu.edu.cn)

This work was supported in part by the National Natural Science Foundation of China under Grant 82001781, and in part by the Science and Technology Foundation of Liaoning Provincial under Grant 2023 MSBA-096.

This work involved human subjects or animals in its research. Approval of all ethical and experimental procedures and protocols was granted by the Ethics Committee of Shengjing Hospital of China Medical University under Application No. 2021PS881K, and performed in line with the Declaration of Helsinki.

ABSTRACT Ovarian cancer is one of the three most common types of gynecological cancer globally, with high-grade serous ovarian cancer being the most common and aggressive histological type. Guided treatment of high-grade serous ovarian cancer typically involves platinum-based combination chemotherapy, necessitating the assessment of whether the patient is platinum resistant. This study proposes a deep learning-based method to determine whether a patient is platinum resistant using multimodal positron emission tomography/computed tomography images. In total, 289 patients with high-grade serous ovarian cancer were included in this study. An end-to-end Squeeze-Excitation–Spatial Pyramid Pooling–Dense Convolutional Network model was built by adding a Squeeze-Excitation Block and Spatial Pyramid Pooling Layer to a Dense Convolutional Network. Multimodal data from positron emission tomography/computed tomography images of regions of interest were used to predict platinum resistance in patients. Through five-fold cross-validation, the Squeeze-Excitation–Spatial Pyramid Pooling–Dense Convolutional Network achieved a high accuracy rate and area under the curve of 92.6% and 0.93, respectively, for predicting platinum resistance in patients. The importance of incorporating the Squeeze-Excitation Block and Spatial Pyramid Pooling Layer into the deep learning model and considering multimodal data was substantiated by performing ablation studies and experiments with single-modality data. The classification results indicate that our proposed deep learning framework performs better in predicting platinum resistance in patients, which can help gynecologists make more appropriate treatment decisions.

INDEX TERMS CNN, ovarian cancer, PET/CT, platinum resistance, SE Block, SPP Layer.

I. INTRODUCTION

Ovarian cancer is the third most common type of gynecological cancer worldwide, with approximately 313,959 new cases and 207,252 deaths, ranking eighth in incidence and mortality among female cancers worldwide [1]. There are five main histological types of ovarian cancer, of which high-grade serous ovarian cancer (HGSOC) is the most common and aggressive histologic type [2]. Treatment guidelines for HGSOC have been suggested by the National Comprehensive Cancer Network, which involves the removal of the tumor followed by platinum-based combination chemotherapy [3]. However, because some patients are resistant to chemotherapy, they are at high risk of recurrence and require

The associate editor coordinating the review of this manuscript and approving it for publication was Hengyong Yu.

further treatment. Generally, the indicator of whether a patient is resistant or sensitive to subsequent platinum-based chemotherapy is based on the length of the platinum-free interval, which is defined as the time interval between the completion of platinum-based combination chemotherapy and disease progression [4]. After initial treatment, patients are considered ''platinum-sensitive'' if they relapse after 6 months or more and ''platinum-resistant'' if they relapse within 6 months. Patients who are platinum-resistant typically have a low response rate to subsequent chemotherapy ($<$15%), with a progression-free survival of 3-4 months and a median survival of $<$12 months [5].

Despite great advancements in precision medicine, proactively and accurately predicting whether a patient is platinum-resistant remains a challenge. If a patient is likely to be platinum-resistant, it is possible to treat the patient more effectively than the standard of care involving platinum-based combination chemotherapy. For example, the approach and timing of surgery can be optimized for secondary cytoreductive surgery, thereby limiting the development of a drug-resistant subclonal tumor population [6]. Simultaneously, patients with drug-resistance can be tested more frequently to detect tumor recurrence without delay. In addition, platinum resistance is a simple indicator of sensitivity to poly (ADP-ribose) polymerase inhibitors [7]. Hence, accurate prediction of platinum resistance in patients reduces the need for unnecessary and cumbersome clinical testing. Therefore, if patients with platinum resistance are accurately identified, they can take full advantage of the benefits of precision medicine.

Currently, most methods for predicting platinum resistance use biomarkers, expression of specific genes or proteins, and tumor immunohistochemistry. Kuhlmann et al. predicted platinum resistance in patients with ovarian cancer using excision repair cross-complementation group 1-positive circulating tumor cells as a predictive biomarker of platinum resistance [8]. Wu et al. found that the risk of platinum resistance was 60-fold higher in patients with high co-expression levels of glutathione peroxidase (GPX4) and cystine/glutamate antiporter solute carrier family 7, membrane 11 (SLC7A11) than in those with low co-expression levels [9]. They determined platinum resistance by assessing whether patients had high co-expression of GPX4 and SLC7A11. However, these methods are associated with high costs, invasiveness, and additional time delays. In contrast, in this study, we adopted 18F-2-fluoro-2-deoxy-D-glucose (18F-FDG) positron emission tomography (PET)/computed tomography (CT), which can non-invasively and more effectively obtain basic information about the tumor, such as the size and location of the primary and metastatic lesions, and used the images to determine whether the patient had platinum resistance. This eliminates the labor-intensive process of manual extraction and detection required by traditional methods, as well as the impact of operator error.

Herein, we propose a deep learning-based approach to predict the presence of platinum resistance in patients using PET/CT medical images. To the best of our knowledge, this is the first use of PET/CT medical images for this purpose. Our method offers improved detection efficiency compared to that by conventional approaches because it follows an end-to-end workflow. Ablation studies demonstrate that the proposed deep learning model can improve the classification accuracy by integrating the Squeeze-Excitation (SE) Block and Spatial Pyramid Pooling (SPP) Layer to prioritize and pool important information at multiple levels. A comparison of single- and multi-modality studies has demonstrated the importance of PET images. Ultimately, the Dense Convolutional Network (DenseNet) model with the SE Block and SPP Layer (SE–SPP–DenseNet) demonstrated the highest precision for predicting platinum resistance in patients.

II. METHODS

A. PATIENTS

This retrospective study was approved by the Radiology Review Committee of the Sheng Jing Hospital of China Medical University and adhered to the principles and requirements of the Declaration of Helsinki. The requirement for further consent was waived. This study involved a retrospective analysis of prospectively collected data from 289 patients with high-grade plasma ovarian cancer who were admitted to our hospital between January 2013 and December 2017.

B. PET/CT DATA

Patients who had fasted and refrained from food and drinking for more than 6 hours were administered a 1-hour intravenous infusion of 161-361 MBq of 18F-FDG before undergoing PET/CT scanning (GE Discovery; GE Healthcare, Inc. Milwaukee, WI, USA). A three-dimensional PET model with a matrix size of 512×512 and an exposure time of 2 minutes per bed was utilized. Following attenuation correction with CT (120 kV, 80 mA), the PET images were reconstructed using a time-of-flight and point-spread function algorithm that incorporated two iterations and 20 subsets.

C. DATA PREPARATION

In our study, physicians delineated the regions of interest (ROIs) in the PET and CT images of the patients. The image data were imported into MATLAB 2021b (MathWorks, Natick, MA, USA), and the ROIs were extracted and stacked into two-dimensional data for each channel. The resulting data were used as inputs for the deep learning network. The data preparation process is illustrated in Fig. 1. The extracted ROIs are shown in Fig. 2 (a) for platinum-sensitive tumors and (b) for platinum-resistant tumors. For each tumors type, two cases are represented with two different ROIs. The left and right ROIs correspond to CT and PET images, respectively.

D. DEEP LEARNING MODELS FOR AUTOMATIC PLATINUM RESISTANCE DETECTION

The deep learning models used in this study were implemented using the Pytorch framework and Python 3.10

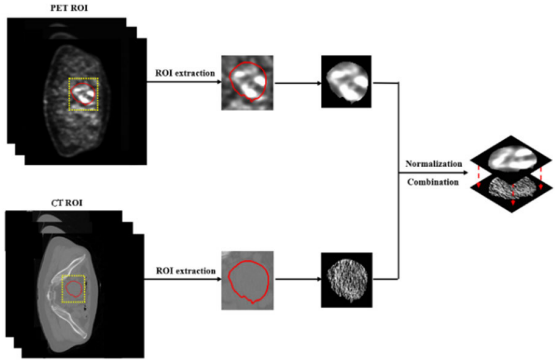

FIGURE 1. Data preparation process.

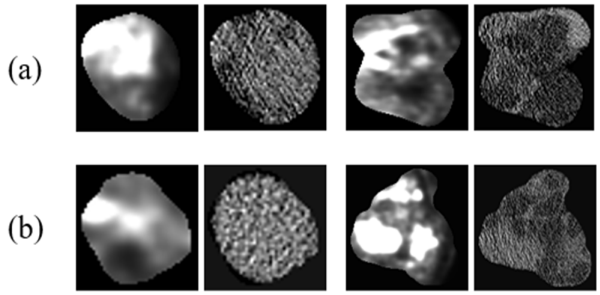

FIGURE 2. Extracted ROIs: (a) ROIs for platinum-sensitive tumors; (b) ROIs for platinum-resistant tumors.

(Python Software Foundation, Fredericksburg, VA, USA) and were trained on a single workstation with an Intel Core i9-13900H processor (Santa Clara, CA, USA), NVIDIA 4060 graphics card (Santa Clara, CA, USA), and 8 GB of random-access memory.

In this study, we constructed a classification model utilizing SE–SPP–DenseNet models to ascertain the presence of platinum resistance by analyzing patient imaging data. A significant difference in the number of patients with platinum resistance (97) and patients with platinum sensitivity (192) would have resulted in an overfitting of the model. Thus, data augmentation was performed on the data of patients with platinum-resistance. Then, the data were rotated by 90° to double their volume, ensuring a relative balance with the data of patients with platinum sensitivity. The dataset was allocated on a per-patient basis in the ratio of training set: validation set: test set = 0.8:0.1:0.1. After assignment, the training, validation, and test sets consisted of 3400 430, and 430, respectively.

We used DenseNet, the structure of which is shown in Fig. 3 [10]. There are four variants of DenseNet models: DenseNet121, DenseNet169, DenseNet201, and DenseNet264. In this study, we used DenseNet121 as the backbone of the convolutional neural network architecture, and we added an SE Block [11] and SPP Layer for prediction. The structure of the SE Block is shown in Fig. 3, in which a four-step operation was performed between the inputs and outputs of the convolutional layers in the network.

We incorporated the SPP Layer into the network, replacing the subsequent pooling layer in the DenseNet output. The SPP Layer was implemented in three steps. First, the input feature maps were pooled using kernels of different sizes to obtain various output feature maps. Second, a fixed-size feature vector was obtained by merging the output feature maps of different sizes. Finally, the feature vector was fed into the fully connected layer for classification. This enabled the extraction of multiscale features and inputted them into a fully connected layer with a fixed size, regardless of the image input size, after selecting suitable spatial bins. Notably, the generated experimental images were resized to 224 × 224 pixels.

We also used a more common deep residual network (ResNet)18 for medical-image classification [12]. The ResNet18 model increases the number of network layers to extract richer features at different depths. Simultaneously, ResNet18 prevents gradient dispersion or gradient explosion by regularizing the initial and intermediate regularization layers. The network structure of ResNet18 is shown in Fig. 4. In this study, we also added the SE Block and SPP Layer to ResNet18. The SE Block was applied to each convolutional block, and its output was used as the input for the next convolutional block. The SPP Layer replaces the Global Average Pooling layer in the ResNet18 model, and its output is classified by the fully connected layer.

Furthermore, we utilized a Swin Transformer model for classification [13]. This model employs a hierarchical construction approach and incorporates a sliding-window mechanism, which allows it to gather information from multiple windows [14]. Its structure is illustrated in Fig. 5.

In our study, the Patch Partition Block down-samples images 4, 8, and 16 times. This approach facilitates target classification and enables the model to handle super-resolution images while focusing on both global and local information. The Linear Embedding Layer performs a linear variation of our input two-channel image, and the Patch Merging Layer performs depth doubling and halving of the height and width of the feature maps after image chunking. The Swin Transformer block is a key component of the Swin Transformer model and consists of two structures. The only difference between them is that one uses windowed multihead self-attention and the other uses shifted windowed multihead self-attention.

E. QUANTITATIVE ASSESSMENT METRICS

In this study, the accuracy, sensitivity, specificity, positive predictive value (PPV), and negative predictive value (NPV) of the above three deep learning models for predicting platinum resistance of patients in the test set were calculated, the receiver operating characteristic (ROC) curves and the confusion matrixes were constructed, and the area under the curve (AUC) was calculated.

III. RESULTS

A. PATIENT CHARACTERISTICS

A total of 289 patients were eligible and included in the study, of whom 97 were platinum-resistant and 192 were

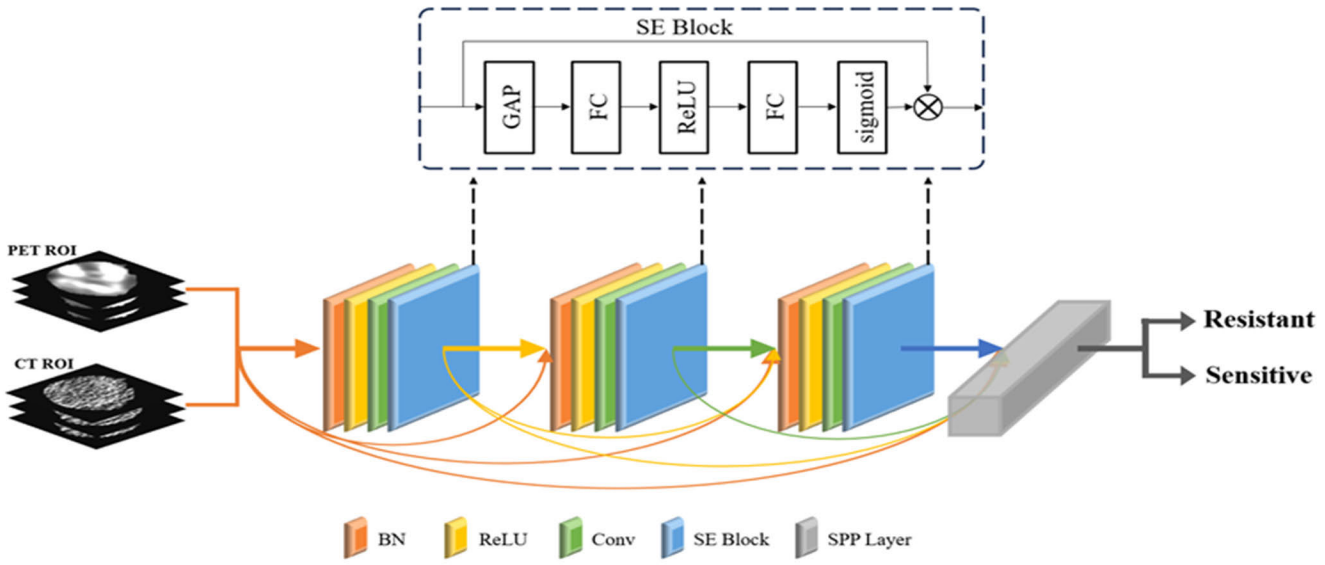

FIGURE 3. Structure of DenseNet.

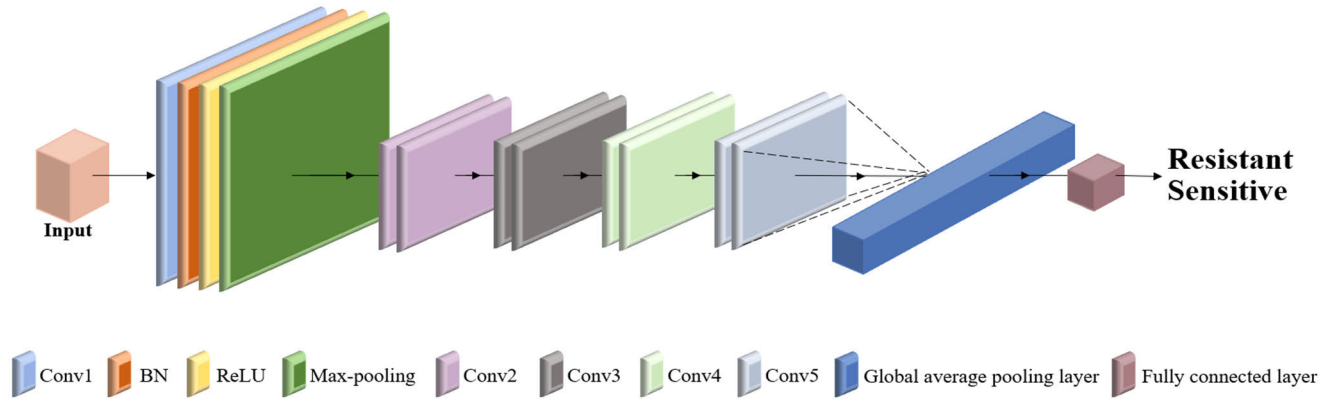

FIGURE 4. Resnet18 network structure.

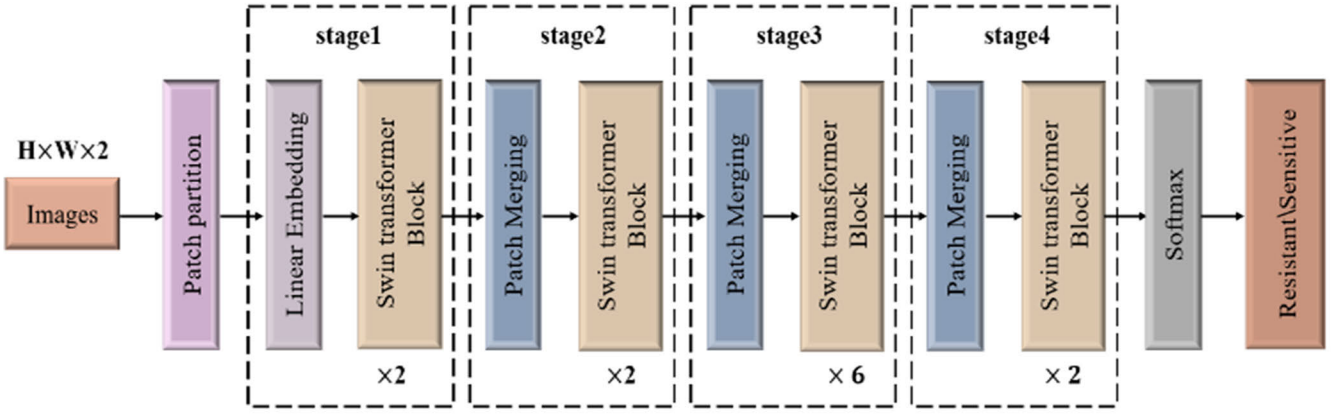

FIGURE 5. Structure of swin transformer.

platinum-sensitive. After data preprocessing and augmentation, the image data of patients with platinum resistance included 4,158 images, and the image data of patients with platinum sensitivity included 4,534 images.

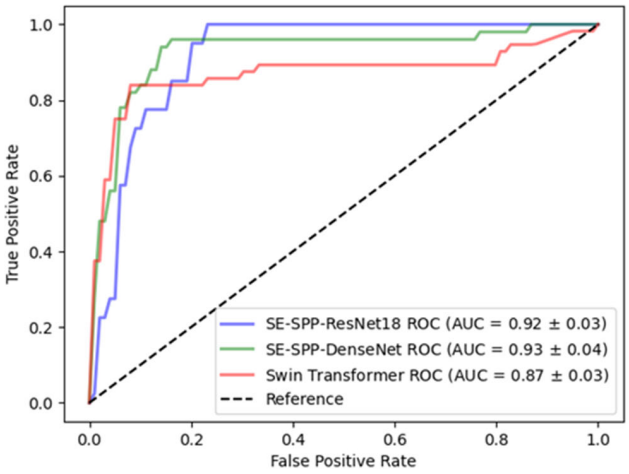

FIGURE 6. ROC curves for classification using PET/CT images with the SE–SPP–DenseNet, SE-SPP-ResNet18, and Swin Transformer models.

B. PARAMETER SETTINGS FOR EACH MODEL

After comparing the results of several preliminary experiments, the specific hyperparameters of the DenseNet, ResNet18, and Swin Transformer models were set, as shown in Table 1.

The learning rate was set to 0.1 times of the original if the loss of the validation set did not decrease after 10 epochs during the training process. In the process of pre-experimentation, we found that all three models could converge before the epoch number was equal to 50. Therefore, we used a fixed epoch number equal to 50 and set the Early Stopping strategy to stop training if the loss of the validation set did not decrease after 20 epochs to prevent the overfitting phenomenon from occurring. Stochastic Gradient Descent (SGD) and binary cross-entropy loss were selected as the network optimizer and loss function, respectively. During the training period, we performed image augmentation, including inversion of the vertical direction of the image and normalization of the image, by calculating the mean and variance of the image. However, it is important to mention that the image augmentation was only performed for the images during the training period, and image augmentation was not performed for the images used for validation and testing.

C. PLATINUM RESISTANCE CLASSIFICATION RESULTS

In this study, a detection framework based on deep learning techniques was proposed to predict whether a patient with HGSOC is platinum-resistant using multimodal images from PET/CT. We investigated the performance of three different deep learning models: DenseNet, ResNet18, and Swin Transformer. The ROC curves of these three models are shown in Fig. 6.

The three models were trained and tested using five-fold cross-validation. The SE–SPP–DenseNet model achieved an accuracy of 92.6%, sensitivity of 86.3%, specificity of 96.1%, PPV of 95.7%, and NPV of 85.7%. Quantitative evaluation of the ResNet18 model, adding the SE Block and SPP Layer (SE–SPP–ResNet18), showed an accuracy of 88.2%, sensitivity of 78.2%, specificity of 95.2%, PPV of 95.8%, and NPV of 75.1%. The Swin Transformer model obtained an accuracy of 83.1%, sensitivity of 85.7%, specificity of 77.5%, PPV of 79.5%, and NPV of 84.2%.

The ROC curves for the three models mentioned above are shown in Fig. 6, where the AUCs of the SE–SPP–DenseNet, SE–SPP–ResNet18, and Swin transformer models were 0.93, 0.92, and 0.87, respectively. The confusion matrices for predicting platinum resistance using the three models are shown in Fig. 7. The SE–SPP–DenseNet had a lower degree of confusion compared to the other two models.

D. EFFECTIVENESS OF SE BLOCK AND SPPLAYER MODULE FOR PLATINUM RESISTANCE ASSESSMENT

We also performed ablation studies to further validate the effectiveness of the SE Block and SPP Layer in improving the prediction performance of the DenseNet and ResNet18 models. The results of the ablation studies are presented in Table 2.

E. THE IMPORTANCE OF PET IMAGES

Furthermore, this study used PET and CT images as multimodal data for training and testing. However, many patients are currently diagnosed using CT alone, and not PET/CT. To illustrate the importance of PET images in predicting platinum resistance, experiments were performed using the three aforementioned models using only CT images for training and testing. The AUCs of the SE–SPP–DenseNet, SE–SPP–ResNet18, and Swin Transformer models were 0.87, 0.84, and 0.64, respectively. The ROC curves and quantitative results for the three models are presented in Table 3 and Fig. 8, respectively.

F. THE MEMORY CONSUMPTION AND TIME EFFICIENCY OF THE DIFFERENT MODELS

To compare the performances of SE–SPP–DenseNet, SE–SPP–ResNet18, and Swin Transformer, we calculated their memory consumption and time efficiency. The results are summarized in Table 4. The SE-SPP-DenseNet had a memory consumption of 645.52 MB and a time efficiency of 0.426 s.

IV. DISCUSSION

In this study, we developed deep learning models to predict platinum resistance in patients with HGSOC. PET/CT images of patients' ovarian cancer lesions were used as two-channel multimodal inputs for prediction using an improved DenseNet model. We improved the accuracy of platinum resistance prediction by adding the SE Block and SPP Layer to the DenseNet model. The SE–SPP–DenseNet model achieved the highest accuracy (92.6%) in predicting platinum resistance.

TABLE 1. Training parameters for the ResNet18, DenseNet, and swin transformer models.

Parameters	Epoch	Learning Rate	Batch Size	Momentum	Weight Decay	Optimizer
ResNet18	50	0.01	64	0.9	0.0001	SGD
DenseNet	50	0.01	48	0.9	0.0001	SGD
Swin Transformer	50	0.001	64	0.9	0.0001	SGD

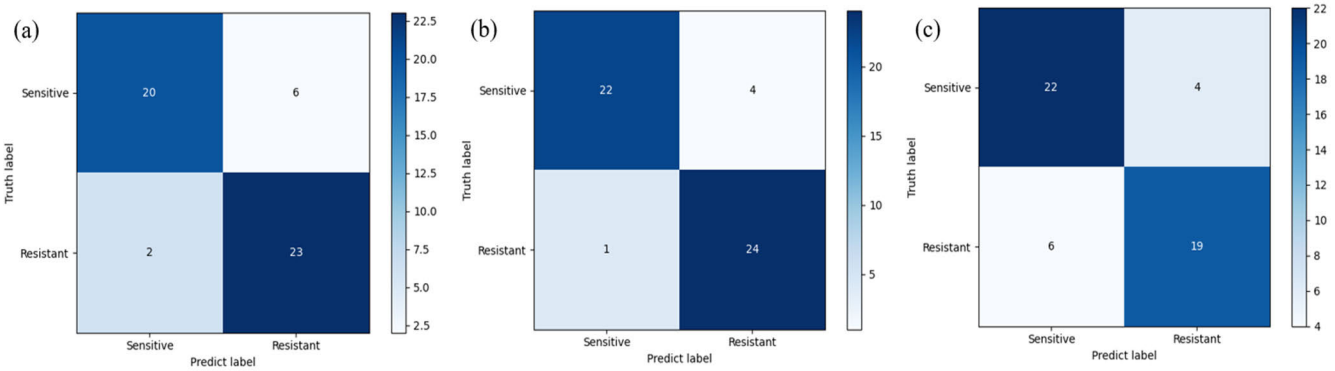

FIGURE 7. Confusion matrices for predicting platinum resistance using three models. (a) SE–SPP–ResNet18, (b) SE–SPP–DenseNet, and (c) Swin Transformer.

TABLE 2. Classification results of ablation studies of the se block and SPP layer in different models.

	Accuracy	Sensitivity	Specificity	PPV	NPV
Resnet18	77.8%	68.2%	78.3%	76.2%	66.7%
Resnet18 + SE Block	82.2%	68.6%	87.5%	89.8%	64.5%
Resnet18 + SPPLayer	84.2%	80.4%	85.1%	85.7%	77.6%
Resnet18 + SE Block + SPPLayer	**88.2%**	**78.2%**	**95.2%**	**95.8%**	**75.1%**
DenseNet	74.3%	73.2%	75.4%	74.5%	73.4%
DenseNet + SE Block	77.2%	76.2%	78.5%	77.4%	75.1%
DenseNet + SPPLayer	83.3%	80.4%	87.5%	88.7%	76.1%
DenseNet + SE Block + SPPLayer	**92.6%**	**86.3%**	**96.1%**	**95.7%**	**85.7%**
Swin Transformer	83.1%	85.7%	77.5%	79.5%	84.2%

From Fig. 6 and Table 2, it is evident that the predictive accuracy of DenseNet surpassed that of ResNet. This is because each DenseNet layer acquires supplementary inputs from all previous layer connections and integrates its own outputs with all subsequent layers. DenseNet is different from ResNet in that it does not simply add the feature outputs of earlier layers to the inputs of later layers but connects these inputs and outputs using fewer parameters. Better classification results can be achieved through dense connectivity between the layers. In addition, the selection of the network should be determined by data complexity.

This study utilized the ResNet18 and DenseNet121 models instead of more complex models, such as ResNet152 and DenseNet264. Although more complex models are expected to achieve better results, they did not perform satisfactorily during training iterations. The models would overfit and become increasingly less accurate soon after the beginning of training. With limited training samples and sample

TABLE 3. Classification results of different models using single modality and multimodality images.

		Accuracy	Sensitivity	Specificity	PPV	NPV
Resnet18 + SE Block + SPPLayer	SM	69.6%	97.6%	39.1%	63.7%	95.0%
	MM	**88.2%**	**78.2%**	**95.2%**	**95.8%**	**75.1%**
DenseNet + SE Block + SPPLayer	SM	76.7%	87.2%	65.2%	73.4%	82.0%
	MM	**92.6%**	**86.3%**	**96.1%**	**95.7%**	**85.7%**
Swin Transformer	SM	61.7%	77.6%	33.9%	56.3%	56.8%
	MM	**83.1%**	**85.7%**	**77.5%**	**79.5%**	**84.2%**

SM = single modality, MM = multimodality

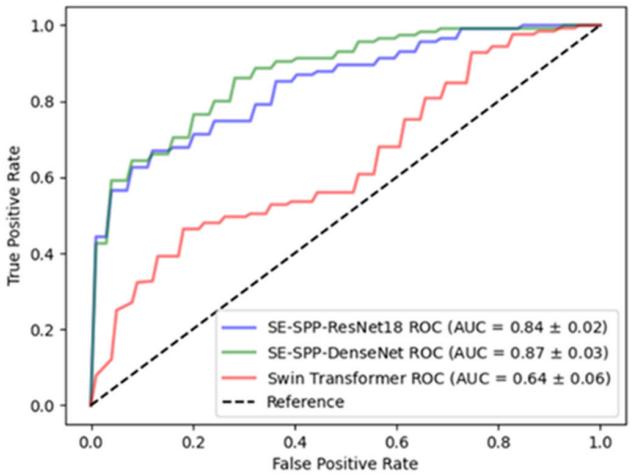

FIGURE 8. ROC curves for classification using CT images with the SE–SPP–DenseNet, SE-SPP-ResNet18, and Swin Transformer models.

TABLE 4. Memory consumption and time efficiency of SE–SPP–DenseNet, SE–SPP–ResNet18, and swin transformer.

	Memory Consumption (MB)	Time Efficiency (s)
SE-SPP-ResNet18	129.91	0.111
SE-SPP-DenseNet	645.52	0.426
Swin Transformer	1017.53	0.446

complexity, increasing the complexity of the model may decrease its fitting ability. However, it can also lead to overfitting and reduce its ability to generalize. The optimal solution used by the SGD algorithm during training is not a global optimal solution but a local optimal solution. Thus, the more complex the network, the more complex the solution space, resulting in the inability to obtain an optimal solution using SGD.

With the increasing complexity of neural network learning, the amount of stored information increases. Hence, it is more advantageous to focus resources on the critical inputs for the current classification task if the computing power is constrained. Therefore, we added the SE Block, which reduces the focus on other information and, as can also be seen in Table 2, the addition improves the accuracy of the model in terms of predicting the patient's platinum resistance. Furthermore, because of the nonuniformity of ROI sizes, it is necessary to adjust the various ROI input sizes for training and testing according to ROI sizes distribution. The test results can then be used to determine the appropriate ROI size for scaling up and down. The SPP Layer not only enables the network to adapt to different sizes of input data but also handles object distortion and spatial layout variations through multilevel pooling, thus improving classification accuracy [16]. Therefore, the SPP Layer was added to the model. As shown in Table 2, the model exhibited an improvement in the quantitative assessment index of platinum resistance in patients after the addition of the SPP Layer.

According to Fig. 7, SE-SPP-DenseNet demonstrated the best classification performance and exhibited the least confusion among the three models evaluated. Table 4 reports the memory consumption and time efficiency of the SE–SPP–DenseNet, SE–SPP–ResNet18, and Swin Transformer models. While the SE-SPP-ResNet18 model offers benefits in terms of memory consumption and time efficiency, its accuracy significantly lags behind that of the SE-SPP-DenseNet. SE–SPP–DenseNet exhibited the highest accuracy and AUC, although it was midstream in terms of memory consumption and time efficiency. Therefore, it can be concluded that SE–SPP–DenseNet is the best-performing model among the three. In addition, we analyzed classification failures and discovered that the majority were due to the ROI being too small, as well as the region occupied by the tumor in the PET images being small. ROIs with small areas were from the top and bottom ends of the tumor or from small tumors. The presence of a small area of the tumor in the PET image may be attributed to physicians sometimes having labeling bias.

Compared to the currently available learning models for predicting platinum resistance in patients, our study

had a different predictive approach and incorporated further improvements. Hwangbo et al. developed a machine learning model to predict platinum resistance in patients using three machine learning algorithms: logistic regression, random forest, and support vector machine [15]. In our study, the SE–SPP–DenseNet model was established to predict platinum resistance in patients using deep learning, which has better model generalization ability than that in machine learning and can extract and learn features directly from raw data, thus simplifying the need to collect relevant features related to platinum resistance in the process of machine learning. This significantly reduces the unnecessary work required in medical imaging applications.

Han et al. used a deep learning model to predict platinum resistance in patients with HGSOC and achieved a classification accuracy of 74% [17]. Liu et al. predicted platinum resistance in patients based on histopathological images using the Inception V3 deep learning model and achieved an AUC of 0.846 for classification [18]. Compared with the above models, our study proposes the SE–SPP–DenseNet model as a superior method for predicting platinum resistance in patients. Wu et al. were able to predict the risk of platinum resistance in patients based on the level of protein expression, but they were still unable to accurately identify the patients [9]. Therefore, the development of a deep learning model based on PET/CT images to predict platinum resistance in patients with HGSOC can help physicians make the most appropriate treatment decisions.

Our study had several limitations. First, as this was a retrospective study, only patient cases within the 4-year timeframe were selected as experimental data, potentially introducing bias in the results. Second, the study's applicability is limited owing to the small sample size, thus requiring an increase in data collection for future research. In the future, we will analyze the association between ROI size and classification results. Furthermore, we can explore the use of segmentation algorithms to automatically identify tumor regions in the PET images of patients with ovarian cancer, thereby reducing the likelihood of human error.

V. CONCLUSION

In this study, we proposed a method using the deep learning model SE–SPP–DenseNet to predict platinum resistance in patients based on multimodal PET/CT images of the ROI. Ablation studies demonstrated that the incorporation of the SE Block and SPP Layer into DenseNet enhanced the classification performance of the original model. Experiments utilizing single-modality CT images demonstrated the importance of multimodal imaging in predicting platinum resistance. The SE–SPP–DenseNet model accurately predicted platinum resistance in patients with a final accuracy of 92.6% and an AUC of 0.93. We believe that gynecologists can use this model for assisted diagnosis to determine the most appropriate treatment plan and prognostic measures based on whether a patient has platinum resistance.

REFERENCES

[1] H. Sung, J. Ferlay, R. L. Siegel, M. Laversanne, I. Soerjomataram, A. Jemal, and F. Bray, "Global cancer statistics 2020: GLOBOCAN estimates of incidence and mortality worldwide for 36 cancers in 185 countries," *CA, A Cancer J. Clinicians*, vol. 71, no. 3, pp. 209–249, May 2021.

[2] G. C. Jayson, E. C. Kohn, H. C. Kitchener, and J. A. Ledermann, "Ovarian cancer," *Lancet*, vol. 384, no. 9951, pp. 1376–1388, 2014.

[3] (2020). *National Comprehensive Cancer Network Clinical Practice Guidelines in Oncology. Ovarian Cancer Including Fallopian Tube Cancer and Primary Peritoneal Cancer, Version 2.* [Online]. Available: https://www.nccn.org/professionals/physician_gls/pdf/ovarian.pdf

[4] M. Friedlander, E. Trimble, A. Tinker, D. Alberts, E. Avall-Lundqvist, M. Brady, P. Harter, S. Pignata, E. Pujade-Lauraine, and J. Sehouli, "Clinical trials in recurrent ovarian cancer," *Int. J. Gynecologic Cancer*, vol. 21, no. 4, pp. 771–775, 2011.

[5] A. Davis, A. V. Tinker, and M. Friedlander, "'Platinum resistant' ovarian cancer: What is it, who to treat and how to measure benefit?" *Gynecologic Oncol.*, vol. 133, no. 3, pp. 624–631, 2014.

[6] A. D. Bois, J. Sehouli, I. Vergote, G. Ferron, A. Reuss, W. Meier, S. Greggi, P. T. Jensen, F. Selle, F. Guyon, C. Pomel, F. Lecuru, R. Zang, E. Avall-Lundqvist, J.-W. Kim, J. Ponce, F. Raspagliesi, S. Ghaem-Maghami, A. Reinthaller, and P. Harter, "Randomized phase III study to evaluate the impact of secondary cytoreductive surgery in recurrent ovarian cancer: Final analysis of AGO DESKTOP III/ENGOT-ov20," *J. Clin. Oncol.*, vol. 38, no. 15_suppl, p. 6000, 2020.

[7] S. A. Cook and A. V. Tinker, "PARP inhibitors and the evolving landscape of ovarian cancer management: A review," *BioDrugs*, vol. 33, no. 3, pp. 255–273, Jun. 2019.

[8] J. D. Kuhlmann, P. Wimberger, A. Bankfalvi, T. Keller, S. Schöler, B. Aktas, P. Buderath, S. Hauch, F. Otterbach, R. Kimmig, and S. Kasimir-Bauer, "ERCC1-positive circulating tumor cells in the blood of ovarian cancer patients as a predictive biomarker for platinum resistance," *Clin. Chem.*, vol. 60, no. 10, pp. 1282–1289, Oct. 2014.

[9] X. Wu, S. Shen, J. Qin, W. Fei, F. Fan, J. Gu, T. Shen, T. Zhang, and X. Cheng, "High co-expression of SLC7A11 and GPX4 as a predictor of platinum resistance and poor prognosis in patients with epithelial ovarian cancer," *BJOG, Int. J. Obstetrics Gynaecol.*, vol. 129, no. 2, pp. 40–49, Nov. 2022.

[10] G. Huang, Z. Liu, L. Van Der Maaten, and K. Q. Weinberger, "Densely connected convolutional networks," in *Proc. IEEE Conf. Comput. Vis. Pattern Recognit.*, Jul. 2017, pp. 4700–4708.

[11] J. Hu, L. Shen, and G. Sun, "Squeeze-and-excitation networks," in *Proc. IEEE Conf. Comput. Vis. Pattern Recognit.*, Jun. 2018, pp. 7132–7141.

[12] K. He, X. Zhang, S. Ren, and J. Sun, "Deep residual learning for image recognition," in *Proc. IEEE Conf. Comput. Vis. Pattern Recognit.*, Jun. 2016, pp. 770–778.

[13] Z. Liu, Y. Lin, Y. Cao, H. Hu, Y. Wei, Z. Zhang, S. Lin, and B. Guo, "Swin transformer: Hierarchical vision transformer using shifted windows," in *Proc. IEEE/CVF Int. Conf. Comput. Vis.*, Jun. 2021, pp. 10012–10022.

[14] X. Xu, Z. Feng, C. Cao, M. Li, J. Wu, Z. Wu, Y. Shang, and S. Ye, "An improved swin transformer-based model for remote sensing object detection and instance segmentation," *Remote Sens.*, vol. 13, no. 23, p. 4779, Nov. 2021.

[15] S. Hwangbo, S. I. Kim, J.-H. Kim, K. J. Eoh, C. Lee, Y. T. Kim, D.-S. Suh, T. Park, and Y. S. Song, "Development of machine learning models to predict platinum sensitivity of high-grade serous ovarian carcinoma," *Cancers*, vol. 13, no. 8, p. 1875, Apr. 2021.

[16] K. He, X. Zhang, S. Ren, and J. Sun, "Spatial pyramid pooling in deep convolutional networks for visual recognition," *IEEE Trans. Pattern Anal. Mach. Intell.*, vol. 37, no. 9, pp. 1904–1916, Sep. 2015.

[17] K. Han, H. Ham, S. I. Kim, Y. S. Song, T. Park, and T. Ahn, "Ensemble of deep learning models to predict platinum resistance in high grade serous ovarian cancer," *Int. J. Data Mining Bioinf.*, vol. 24, no. 3, pp. 220–237, 2020.

[18] Y. Liu, B. Lawson, X. Huang, B. Broom, and J. Weinstein, "RETRACTED: Prediction of ovarian cancer response to therapy based on deep learning analysis of histopathology images," *Cancers*, vol. 15, no. 16, p. 4044, Aug. 2023.

HAOMING ZHUANG is currently pursuing the master's degree with the College of Medicine and Biological Information Engineering, Northeastern University. His research interests include medical image analysis and deep learning.

BEIBEI LI is currently a Medical Professional with Shengjing Hospital of China Medical University, specializes in the field of imaging medicine and nuclear medicine. Her research interests include imaging diagnosis of ovarian tumors and the utilization of artificial intelligence in the realm of medical imaging.

JINGTONG MA is currently pursuing the bachelor's degree in intelligent medical engineering from the College of Medicine and Biological Information Engineering, Northeastern University. Her research interests include biomaterials, microfluidic analysis, and the analysis of medical images based on deep learning.

PATRICE MONKAM is currently an Assistant Professor with Northeastern University, China. His current research interests include image processing and analysis, medical imaging, deep learning, and its applications.

WEI QIAN is currently a Professor with Northeastern University, China. His research interests include biomedical imaging and image processing. He is a fellow of the American Institute for Medical and Biological Engineering (AIMBE).

DIANNING HE is currently an Assistant Professor with Northeastern University, China. His current research interests include analysis methods of medical image and intelligent diagnosis of cancer.